sustainability

MDPI

Article

Physical Separation of Contaminated Soil Using a Washing Ejector Based on Hydrodynamic Cavitation

Kanghee Cho [1], Hyunsoo Kim [2], Oyunbileg Purev [2], Nagchoul Choi [1,*] and Jaewon Lee [3]

[1] Research Institute of Agriculture and Life Sciences, Seoul National University, Seoul 08826, Korea; kanghee1226@snu.ac.kr
[2] Department of Energy and Resource Engineering, Chosun University, Gwangju 61452, Korea; star8538@naver.com (H.K.); oyunbileg@chosun.kr (O.P.)
[3] JIU Corporation, Seoul 07528, Korea; jaewlee@jiuene.com
* Correspondence: nagchoul@snu.ac.kr

Abstract: A washing ejector is a pre-treatment technology used to remediate contaminated soil by separating fine particles. The washing ejector developed in this study is a device that utilizes fast liquid jets to disperse soil aggregates by cavitation flow. The cavitation phenomenon is affected by the Bernoulli principle, and the liquid pressure decreases with the increase in kinetic energy. The cavitating flow of the fluid through the Ventrui nozzle can remove surface functional groups and discrete particles. The main methodology involves the removal of small particles bound to coarse particles and the dispersion of soil aggregates. Particle collisions occur on the surface soil, such as the metal phase that is weakly bound to silicate minerals. It was observed that the dispersed soil affected the binding of toxic heavy metals and the mineralogical characteristics of the soil. The quantity of oxides, organic matter, and clay minerals affected the properties of the soil. An almost 40–60% removal efficiency of total metals (As, Zn, and Pb) was obtained from the contaminated soils. After treatment by a washing ejector, the volume of fine particles was reduced by 28–47%. When the contaminants are associated with particulates, separation using a washing ejector can be more effective. Therefore, physical separation improves the removal efficiency of heavy metals from soil aggregates.

Keywords: washing ejector; cavitation; physical separation; remediation; heavy metals

Citation: Cho, K.; Kim, H.; Purev, O.; Choi, N.; Lee, J. Physical Separation of Contaminated Soil Using a Washing Ejector Based on Hydrodynamic Cavitation. *Sustainability* **2022**, *14*, 252. https://doi.org/10.3390/su14010252

Academic Editor: Franco Ajmone Marsan

Received: 18 November 2021
Accepted: 24 December 2021
Published: 27 December 2021

1. Introduction

Soil contaminated with toxic heavy metals is a major environmental concern in several countries. The emission of fine dust particles from the smelting of non-ferrous metals is a notable environmental issue [1,2]. These contaminants are fine (<2 μm) or ultrafine (<0.5 μm) particles that mainly include slag fragments and un-melted ore [3]. Furthermore, fine dust particles pollute surface soils based on the direction of the wind and negatively affect the health of local populations [4,5]. Soils near smelters accumulate contaminants and can be analyzed to investigate the long-term effects of metal contaminants on soils [6]. The accumulation of metals is significantly affected by the contents of organic matter, clay minerals, and Fe oxides in the soil [7]. Generally, fine soil fractions can adsorb more contaminants than coarse soil fractions through various complexation reactions because of their higher surface-to-mass ratios [8]. Therefore, the content of toxic heavy metals in the soil increases with decreasing particle size, and it is harder to remove contaminants from fine soil fractions. The oxides produced by Si–OH and Al–OH can act as adsorption sites for toxic heavy metals [9]. Fe oxides in fine soil provide adsorption sites for anion species on the reactive surfaces [10].

Soil that has been contaminated with smelting-related contaminants is treated via various techniques, such as soil washing, solidification/stabilization, and phytoremediation. Among these techniques, soil washing is often the preferred choice; it can be used to treat

a wide range of toxic metals and reduce the cost and time of the remediation [11–13]. However, post-treatment remains necessary to ensure soil quality. For example, soil washing with a solution that has high dissolution strength may be preferred for soil with a high proportion of fine particles, even though strong reagents could adversely affect the quality of the soil [14]. Previous studies have shown the effects of several parameters (e.g., washing time, stirring speed, and soil-to-water ratio) on the removal efficiency using various washing solutions, such as acids and alkalis. However, soil washing consumes a large amount of washing agent and produces large amounts of wastewater, resulting in post-processing issues and increased cost-of-treatment. Therefore, contaminated soil with smelting-related contaminants requires suitable pre-treatment to avoid secondary pollution and low-cost treatment [15]. From a field application perspective, developing efficient pre-treatment is necessary for contaminant removal in soil, which could not only improve cost efficiency but also save resources and energy.

The volume of the contaminants can be correlated to the fine-particle distribution in the soil [16]. Physical separation can be performed for the remediation of contaminated soil and sediments. These methods used for particle distinction include screening, hydrodynamic classification, density (or gravity, float-sink) separation, froth flotation, magnetic separation, and attrition scrubbing [17]. Integrated processes that combine both physical and chemical methods were followed along with soil washing to enhance the efficiency of the extraction [18]. However, small particles that are bound to coarse particles hamper the overall effectiveness of soil washing. This is caused by the contained organic matter and soil mineral components (e.g., oxides). The removal efficiency of contaminants depends on the form of the particles (size and surface properties), which are governed by the soil properties [19]. According to the literature [20], As forms are found in small soil particles with colloidal properties (e.g., Fe oxide minerals), which implies the effect of soil particle size. Thus, before the treatment of the contaminants, enhanced physical separation of fine particles is necessary along with the surface cleaning of the particles from the contaminated soil. Enhanced separation may improve the removal efficiency of the contaminants post-treatment.

Based on the feature of hydrodynamic cavitation, the washing ejector developed in this study is a device that utilizes high-pressure water to disperse soil aggregates. The cavitation phenomenon is affected by the Bernoulli principle, and the liquid pressure decreases with the increase in kinetic energy [21]. It has been reported that the geometry of Venturi tube causes the cavitation phenomena in water flow. Hydrodynamic cavitation technology has been well documented in the literature and, as a technology with advantages pertaining to energy efficiency, has attracted intense interest [22]. Moreover, hydrodynamic cavitation can be considered a sustainable and easy-to-handle technique. Hydrodynamic cavitation is the formation, growth, and subsequent collapse of microbubbles in aqueous solutions [23]. The collapses also result in the formation of highly reactive free radicals, continuous surface and interface cleaning, as well as the enhancement of mass transfer rates due to generated turbulence [24]. For this reason, studies on cavitation have been applied to mineral processing, chemical reactions, and water purification and have shown remarkable results [25–27]. The washing ejector is based on the principles of physical separation, which is used to separate metal-bearing particles from contaminated soil. In this study, a small-scale washing ejector was utilized to separate fine particles that contained contaminants. Furthermore, we suggest technologies for the removal of the metal phase that is bound to the soil surface.

2. Materials and Methods

2.1. Soil Characterization

The contaminated soil samples were collected from around the smelter located in the village of Seokpo, in Bonghwa County, Gyeongbuk Province, Korea. This site was widely contaminated with toxic heavy metals because of the dust emissions from smelters. In addition, the surrounding areas contain spreads of vegetable farmland, which are located

approximately 2 km away from the smelter. Contaminants associated with particulates emitted from smelting and fuming are concentrated in the ultrafine particle fraction [2]. Moreover, contaminant concentrations in soils near smelters are characterized according to the wind direction. Soil contamination revealed that the surrounding areas in a radius of up to approximately 4 km around the Zn smelter were widely contaminated by heavy metals, including As, Pb, and Zn [4].

The soil samples were air-dried and sieved through a 2 mm sieve. The observed primary physical and chemical properties of the soil were as follows: 8.85 pH and 4.25% organic matter. The main mineralogical constituents of soil are silicate minerals in which SiO_2 (65.8 wt%), Al_2O_3 (17.6 wt%), and Fe_2O_3 (5.33 wt%) are dominant (Table 1). In addition, the mineral composition analysis of the bulk soil using XRD revealed that it consisted of dickite, muscovite, and quartz. The results of the particle size analysis of the bulk soil revealed the following composition: sand (58.4%), silt (27.6%), and clay (14.0%), which represents the textural classification of sandy loam. In addition, 300 g of soils was placed on the top of a nest of sieves and fractionated into four aggregate sizes using a vibrating screen instrument. The soil particle was divided into four fraction sizes, 2–0.5, 0.5–0.25, 0.25–0.075, and <0.075 mm. The distribution of the soil was determined by the weight of each sieve after sieving, which corresponded to 22.5%, 18.7%, 18.8%, and 40.0%, respectively, of the soil sample. In order to apply a small-scale test, optimum cutoff size should be determined considering the size distribution of the soil. Consequently, the cutoff size of the treated soil was set as 0.075 mm considering the loss of fine particles.

Table 1. Soil physicochemical properties.

Soil Physicochemical Property			Major Constituents [1]			
			Compound	wt%	Compound	wt%
pH		8.85	SiO_2	65.8	SO_3	0.99
Organic matter (%)		4.25	Al_2O_3	17.6	Na_2O	0.82
Texture	Sand (%)	58.4	Fe_2O_3	5.33	TiO_2	0.53
	Silt (%)	27.6	K_2O	3.94	ZnO	0.33
	Clay (%)	14.0	CaO	2.75	MnO	0.05
	Classification	Sandy loam	MgO	1.45	As_2O_3	0.02

[1] The content of major constituents was determined using XRF.

2.2. A Washing Ejector Based on Hydrodynamic Cavitation

Cavitation occurs when vapor bubbles form and grow in a liquid medium when the static pressure drops locally below the saturated vapor pressure. Based on the Bernoulli principle, the liquid pressure decreases with an increase in kinetic energy. Because the gravitational effects are negligible under normal conditions, the kinetic energy changes with static pressure [21]. The Bernoulli equation is as follows:

$$P_1 + \frac{\rho_1 V_1^2}{2} = P_2 + \frac{\rho_2 V_2^2}{2} \quad (1)$$

where P_1 and P_2 are the pressures upstream and downstream and ρ_1 and ρ_2 are the densities of the liquid upstream and downstream, respectively. V_1 and V_2 are the liquid flow velocities upstream and downstream, respectively.

Cavitation can be generated by alterations in fluid flow and pressure, which are caused by specific constructions such as Venturi tubes [22]. For the fluid flow through the Venturi tube, the local average velocity accelerated and the local static pressure decreased owing to the reduction in the cross-section of the flow passages. Geometric parameters such as throat diameter and the convergent and divergent angles play a role in the design of a Venturi tube, as these parameters greatly affect cavitational inception [28–31]. Once the cavitational inception is achieved, the pressure falls below or is equal to the vapor pressure of the liquid, which means that some of the energy is utilized for the generation of the

vapor phase [28]. Throat pressure is an indicator of cavitation because bubble nucleation and growth are expected when the throat pressure reaches the vapor pressure [29]. In this respect, the cavitation number is derived from Bernoulli's theorem and plays a crucial role in the intensity of cavitation. The cavitation number (C_v) is a dimensionless parameter that represents the cavitation intensity. The formula for the cavitation number is expressed as [21]:

$$C_v = \frac{P_2 - P_v}{\frac{1}{2}\rho V_0^2} \quad (2)$$

where P_2 is the fully recovered downstream pressure, P_v is the vapor pressure of the liquid at the reference temperature, ρ is the density of the liquid, and V_0 is the velocity of the liquid at the Venturi throat.

A washing ejector is a pre-treatment technology used to remediate contaminated soil by separating fine particles. In these experiments, the fluid used was water. Figure 1a shows a schematic diagram of the washing equipment at small scale. The washing ejector consists of a feeder, a primary nozzle, a mixing chamber, and a diffuser zone as its main parts. Figure 1b shows the cavitating device. Figure 1c presents a visualization of the separation of the soil aggregate in the washing ejector. Cavitation occurs in flowing liquids because hydrodynamic cavitation results in regions where the pressure falls below the vapor pressure [30].

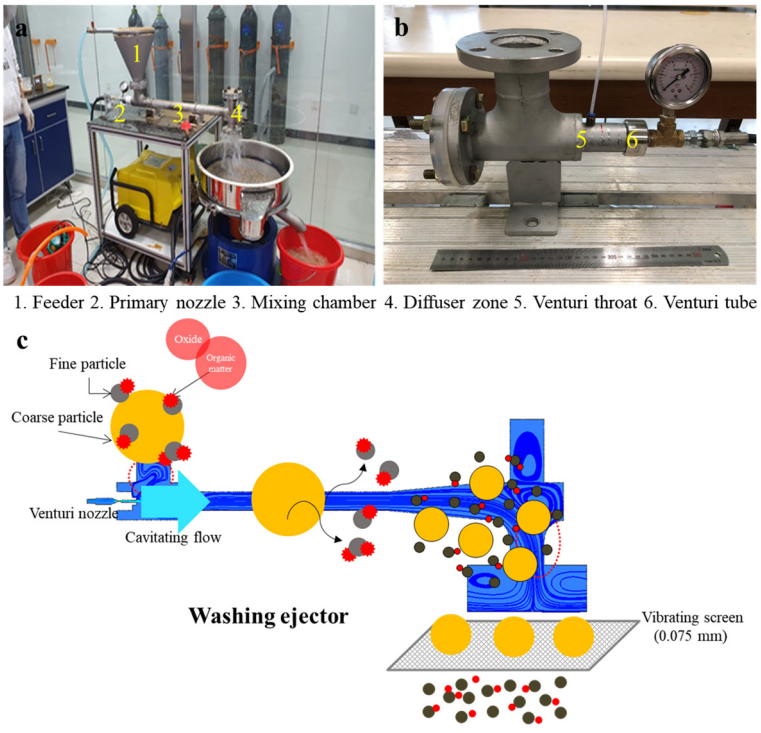

Figure 1. (**a**) The photo of the washing ejector and (**b**) the cavitating device. (**c**) Schematic representation of a washing ejector.

The Venturi nozzle was attached to a cavitating device, which was connected to a washing ejector. The diameter of Venturi tube (D) was 5 mm, and the throat diameter (d) was 3 mm, with a diameter ratio of 2.78. The static pressure at the Venturi throat was measured using a digital pressure gauge (PX409-015GUSBH, Omega Engineering Inc., Norwalk, CA, USA). The feeder was set on the top of the chamber, and the nozzle was parallel to the axis of the ejector. High pressure water was sprayed from the nozzle into the mixing chamber zone, and completely mixed with the soil via the feeder. The mass flow was discharged to a diffuser zone, placed at the end of the ejector. This zone is characterized

by the expansions, collision, and then drop. In particular, collision could take place on the surface soil such as the metal phase weakly bound on surface silicate minerals.

To compare the flow characteristics between the cavitating flow and non-cavitating flow, the separation of fine particles at different inlet pressures under a washing ejector was investigated while using a lower water volume with a liquid-to-solid (L/S) ratio of 2. In Section 3.1, the cavitating flow characterization with respect to different conditions is analyzed. In the present study, the inlet pressure was set at 5 MPa based on the cavitation inception using the characteristics of the cavitating flow. The bulk soil was passed through a 2 mm sieve to remove the gravel, and the sample was put into the feeder. In order to investigate the effect of the separation on the soil for the removal of fine particles, the dispersed soil was screened (0.075 mm) in the vibration screen, and the chemical properties and mineralogical characteristics of the soil were investigated.

2.3. Analysis Method

The pH of the sample was measured at a soil-to-water ratio of 1:5 (*v*/*v*), and the organic matter content was determined using the ignition method (weight loss at 450 °C). The particle size fraction divides soil into three textural fractions of sand, silt, and clay. We performed a particle size distribution analysis according to the ASTM method, D 422-63. In addition, weighted soil was sieved, and soil on each level was collected and weighted using an analytical balance for size distribution investigation. The samples were analyzed via XRD (X'Pert Pro MRD, PANalytical, The Netherlands). Cu–Kα X-rays were used at an acceleration voltage of 40 kV and a current of 30 mA. The sample was analyzed for 2θ values of 10–70° to determine the mineral phase composition. Fourier-transform infrared (FTIR) spectroscopy (Nicolet 6700, Thermo Fisher Scientific, Waltham, MA, USA) was used to analyze the soil. The elemental compositions of the samples were determined using XRF spectrometry (S4 PIONEER, Bruker AXS, Germany). Polished sections were prepared by placing soil in an epoxy resin, which, after curing, was polished to ensure flatness. The morphology of soil samples was analyzed using a field emission scanning electron microscope (FE-SEM, S4800, Hitachi, Tokyo, Japan) with an energy dispersive spectrometer (EDS, ISIS310, Jeol, Tokyo, Japan).

Total heavy metal concentrations were determined in both bulk and treated samples by ICP-OES (Perkin Elmer Optima Model 5300DV, Waltham, MA, USA). The heavy metals in the soil were measured based on the Korean Standard Test methods (aqua regia) and compared to the Korean warning standards for a forest land and residential area. Total concentrations of heavy metals in 1 g soil samples were extracted using HCl and HNO_3 at a 3:1 ratio (i.e., aqua regia), and the extracts were filtered for analysis. The chemical forms of As and Fe in soils were analyzed using the sequential extraction procedure described by Wenzel et al. (2001) [32], which divides As-bound and Fe-bound soil fractions into five fractions (Table A1). The fractionation of the Cd, Cu, Pb, and Zn in the soil was also determined using the traditional sequential extraction method (i.e., Tessier's method) for the standards and measurement [33]. The detailed conditions of sequential extraction procedures are summarized in Appendix A. After each extraction step, the samples were centrifuged at 3000 rpm for 10 min, filtered, and analyzed via ICP-OES.

3. Results

3.1. Characterization of Cavitating Flow by Using a Washing Ejector

To evaluate the characteristics of the cavitating flow using the washing ejector, the inlet pressure was controlled using the flow control valves, ranging from 1 to 5 MPa gauge pressure. The cavitation phenomenon is related to the pressure drop in a flowing liquid through the Venturi tube. In Figure 2, the observed cavitation number decreased from 2.72 at 1 MPa to 0.50 at 5 MPa, indicating that the intensity of cavitation flow increases with an ascending pressure drop at the Venturi throat. The flow rate was 1.3 L/min for an inlet pressure of 1 MPa, 2.6 L/min for 3 MPa, and 3.0 L/min for 5 MPa. With the increase in the inlet pressure, the static pressure difference increases from 0.007 to 0.01 bar. Eventually, the

static pressure affected the cavitating flow in a washing ejector. As can be seen, the gauge pressure ascends as the static pressure difference increases, and the cavitation number was gradually decreased. The experimental results can be observed at a condition cavitation number < 1, which indicates the inception of cavitation [29,30]. These results demonstrated that the static pressure ascends and could promote the inception of cavitation, and the cavitation number is a good estimate of cavitating flow. The experimental results showed reasonable agreement with the CFD results for cavitation behaviors published in the literature [17,23].

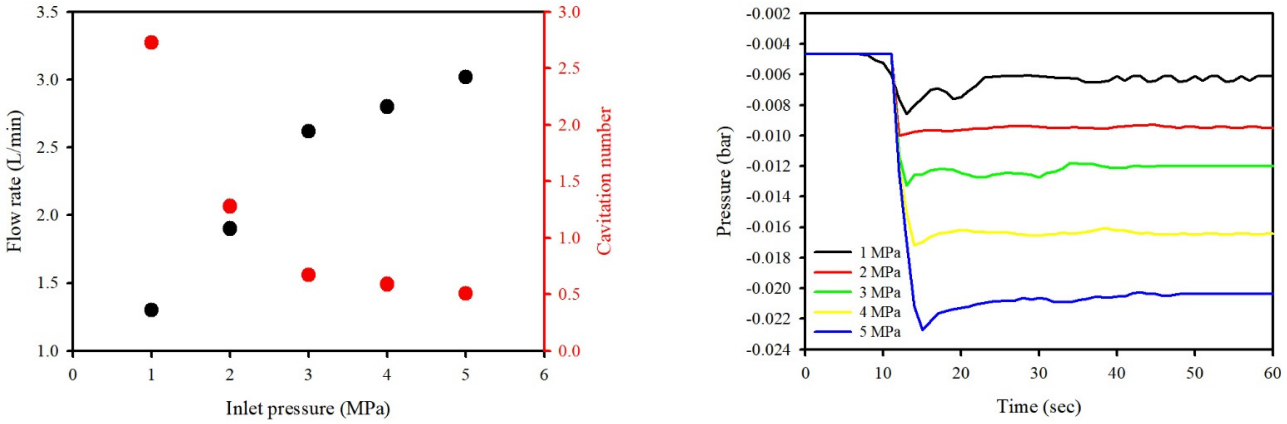

(**a**) (**b**)

Figure 2. The hydrodynamic conditions presented in (**a**) effect of inlet pressure on flow rate and cavitation number, (**b**) time history of the pressure for the Venturi throat.

The soil aggregates contained organic matter and a wide range of particles with different size fractions. The washing ejector was used to compare the size distribution of the dispersed soil particles. In order to investigate the effect of different initial pressures for the removal of fine particles, the dispersed soil was screened (0.075 mm) in the vibration screen. Table 2 shows the weight fraction of coarse particles of dispersed soil, under the fluid pressure of 1, 3 and 5 MPa.

Table 2. Effect of fluid pressure on size distribution of the dispersed soil.

Pressure (MPa)	Weight (%)	
	+0.075 mm	−0.075 mm
1	88.6	11.4
3	87.0	13.0
5	81.1	18.9

The separation efficiency increased with the increasing fluid pressure because the mechanical attrition increased the removal degree of the metal phase that was bound to the soil surface. Under the cavitating flow at 5 MPa, the content of organic matter reduced from 4.25% to 1.45%. After the treatment with the washing ejector, the fine particles (i.e., soil colloids) in the soil aggregates were removed by the high-pressure fluid. Thus, the quantity of fine particles and organic matter in larger-sized particles was reduced, which increased the intensity of the quartz peaks (Figure 3a). In addition, the XRD pattern of the soil revealed the presence of rutile (TiO_2) and wustite (FeO). These minerals were formed by reactions between organic matter, clay minerals, and contaminants [34].

Fourier-transform infrared spectroscopy of the washed soil was conducted after the sample was treated with the washing ejector (Figure 3b), and the spectra revealed an increase in the intensity of the main bands. The spectrum of the original soil sample exhibited bands at 3696, 3619, and 3421 cm^{-1} (O–H stretching); 1636 and 1419 cm^{-1} (C=N

stretching); 1031, 912, 778, 694, and 534 cm^{-1} (Si–O stretching); and 470 cm^{-1} (Fe–O stretching). The Si–O stretching vibration band corresponded to quartz; these quartz bands were prominent in the spectrum of the soil [7]. Furthermore, the peaks at 2917 and 2849 cm^{-1} were ascribed to the asymmetric C–H stretching vibrations (–CH_2 and –CH) in aliphatic hydrocarbons [35], which corresponded to organic matter. Therefore, the fine particles were influenced by organic matter, and the metal phase was likely adsorbed on the surface. The separation produced clean soil surfaces by removing organic matter because the organic matter bands disappeared, and the intensities of the bands caused by the O–H, C=N, and Si–O stretching vibrations increased.

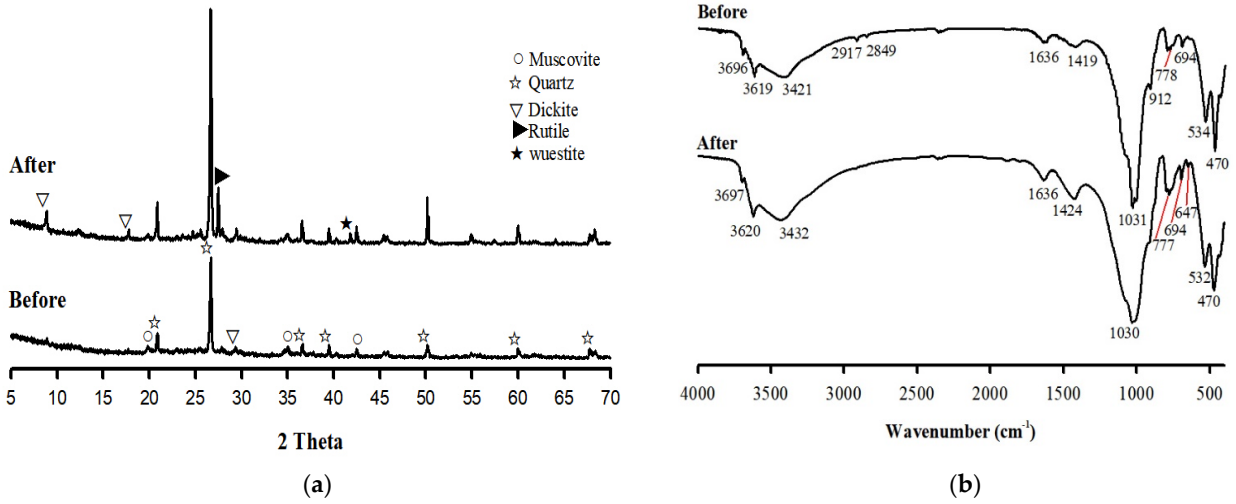

Figure 3. (**a**) XRD patterns and (**b**) FT-IR spectra of the original soil and treated soil.

3.2. Characterization of the Contaminated Soil

The concentrations of toxic heavy metals (As, Cd, Cu, Pb, and Zn) in the soil (Table 3) exceeded the cleanup level of the Korean Soil Environment Conservation Act (KSECA). Zn showed the highest concentration among the measured metals, exceeding the level of KSECA by almost 17 times. The soil was divided into two different particle sizes (±0.075 mm) (Figure 4). The concentrations of Cd, Cu, Pb, and Zn in the fine soil were approximately two times higher than those in the coarse soil. The fine soil particles largely adsorbed the heavy metals because of their higher surface-to-mass ratios. In addition, the total Fe concentrations in bulk, fine, and coarse soils were 26,920, 31,290, and 31,810 mg/kg, respectively.

Table 3. Physicochemical characteristics of the contaminated soil.

Contaminants	Values (mg/kg)	Regulation Level in Korea [1] (mg/kg)
As	135.5 ± 10.7	25
Cd	90.2 ± 8.2	4
Cu	524.6 ± 45.0	150
Pb	613.4 ± 44.8	200
Zn	5034 ± 57.5	300

[1] Concerning level of the Soil Environment Conservation Act of Korea (KSECA) legislated by Korean Ministry of Environment (K-MOE).

A five-step sequential extraction of As and Fe in the soil samples was conducted as described by Wenzel et al. (2001) (Figure 5). As and Fe in the soil were mostly bound to crystalline oxides (Step 4) and as residual phases (Step 5), which indicated that Fe oxides influenced the retention of As in the soil. In particular, the high total concentration of Fe and the presence of residual Fe (Step 5, 60.1%) indicated that Fe oxides in the soil minerals were associated with phyllosilicates, such as dickite and muscovite, or sulfide minerals [36]. As in the soil is mainly adsorbed by Fe oxides rather than by organic matter [19]. In addition, the

colloidal properties of Fe oxide minerals play an important role in holding large amounts of As [20,35]. Sequential extractions (Tessier's method) were also conducted to evaluate the speciation of Cd, Cu, Pb, and Zn in the soil. Cd, Cu, and Zn were mostly bound to carbonates (Step 2), whereas Pb existed predominantly in the residual phase (43.1%) of the soil. This indicated that the Pb compositions were associated with ore fragments and sulfide minerals. Cd, Cu, and Zn in the soil existed predominantly in carbonate fractions, which indicated that they favored high solubility and mobility.

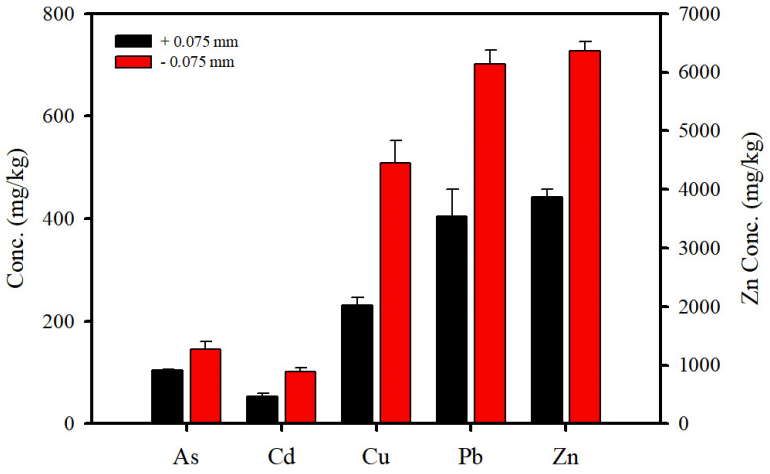

Figure 4. Concentration distribution of toxic heavy metals according to particle size (±0.075 mm).

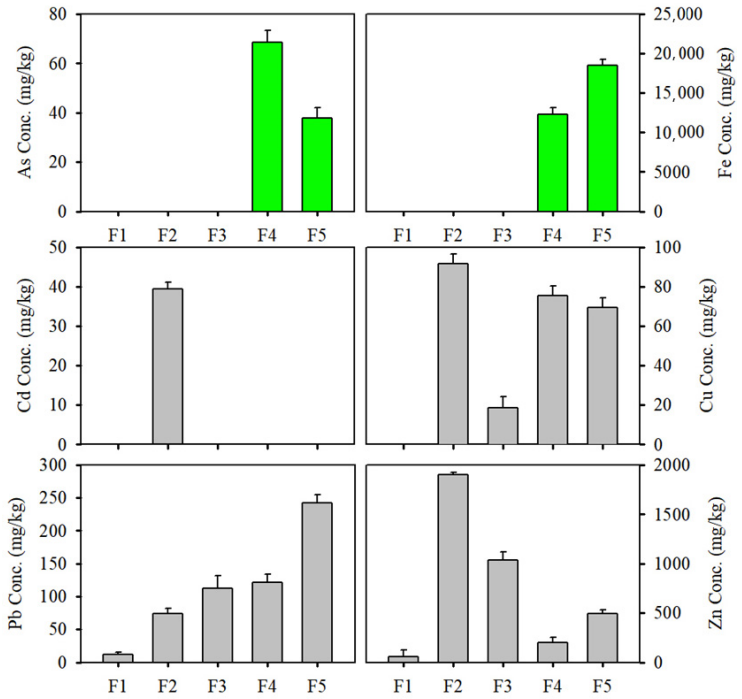

Figure 5. Sequential extracted metal fractions from bulk soil (+0.075 mm). For As and Fe, each fraction represents: (F1) non-specifically sorbed; (F2) specifically sorbed; (F3) amorphous oxide associated; (F4) crystalline oxide associated; (F5) residual. For Cd, Cu, Pb, and Zn, each fraction represents: (F1) exchangeable; (F2) carbonate; (F3) amorphous Fe and Mn hydroxide; (F4) organic matter bound and sulfide; (F5) residual.

SEM observations confirmed the presence of contaminants that are commonly associated with particulates emitted from smelting (Figure 6). SEM-EDS images of metal-bearing particles from bulk soil showed that the soil particles were composed of silicate grains sur-

rounded by amorphous oxides. These particles had subhedral, anhedral, and sheet-shaped morphologies. EDS analysis revealed that the soil particles contained large portions of Al, Si, O, and trace elements (Fe, Mn, S, and Zn). The solid phases were characterized as mixtures of silicate minerals and sulfide minerals. One of these forms was silicate grains surrounded by amorphous toxic heavy metals. Light-gray silicate particles revealed that the Fe oxides and soil aggregates contained phases related to the discrete crystals. Sphalerite (ZnFeS) corresponded to the particles produced by ore processing, and toxic heavy metals were present as secondary phases in the soil, which might have been caused by the weathering of sulfide minerals or the smelting of non-ferrous metal.

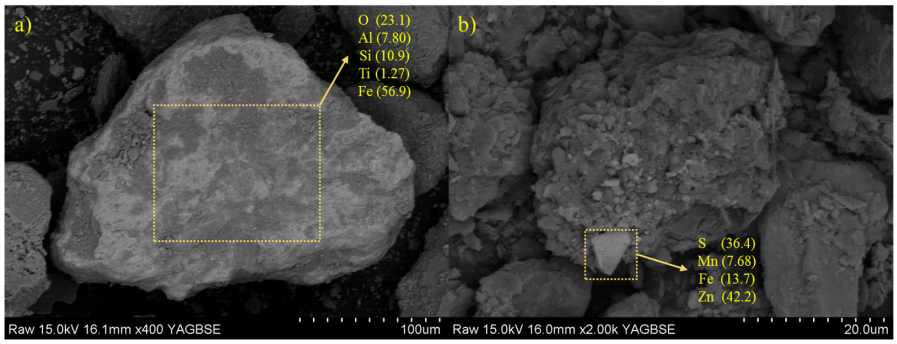

Figure 6. Scanning electron micrographs in backscattered electrons (BSEs) of a bulk soil. (**a**) Soil particle associated with Fe oxide. (**b**) Sphalerite occurred as discrete particles. Element concentrations are expressed in wt%.

In the microscopic image of the polished section (Figure 7a), the mineral phases were observed in the form of quartz. Secondary phase sizes range from <1 to about 30 µm. The microstructure of the polished section, investigated through SEM-EDS analysis (Figure 7b), was composed of metallic oxide phases embedded within the silicate matrix. Metallic oxide phases were visible in back-scattered electron (BSE) images as a white halo on light gray particles. The elemental mapping by EDS shows four different compositional regions of Al, Si, Pb, and O. The focus on the zones with light gray particles indicates that Pb oxides impregnated the space of the silicate grains. These secondary phases were present as discrete euhedral to subhedral grains with irregularly shaped morphologies.

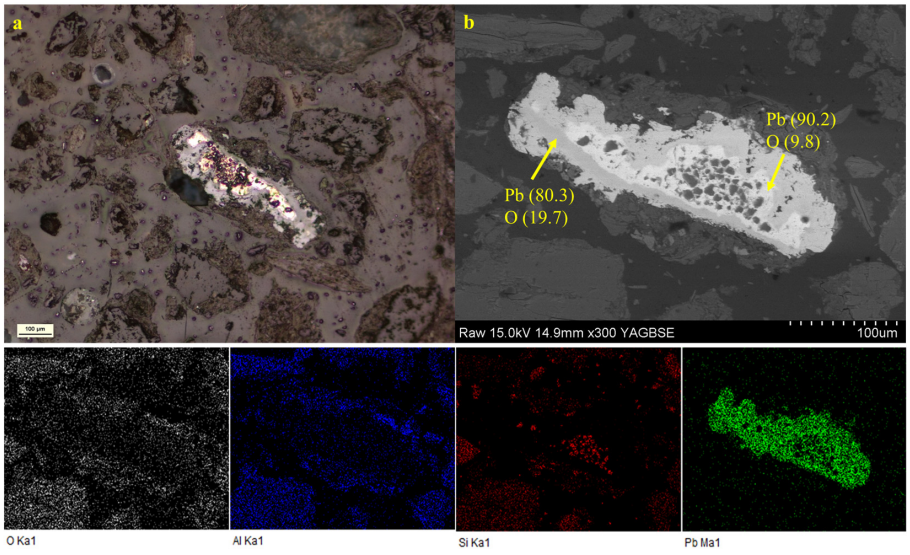

Figure 7. (**a**) Reflected light image of a polished sample on bulk soil. (**b**) Scanning electron micrographs in backscattered electrons (BSEs) of polished sample and EDS mapping. Element concentrations are expressed in wt%.

3.3. Effect of Soil Separation Using a Washing Ejector

Figure 8 shows the removal efficiencies of the toxic heavy metals from the dispersed soil. These removal efficiencies followed the order Cd > Zn > As > Pb > Cu, which indicated that fine particles could affect the removal of toxic heavy metals from the bulk soil. Moreover, the removal efficiency was greatly improved after physical separation. The concentrations of heavy metals in the soil correlated with the soil content in clay minerals, soil organic matter, oxides, and $CaCO_3$ [10,19]. In particular, complex formations between the Fe oxide surface and As species suggested that complexation proceeds via the adsorption of As to the oxide surface [20]. Therefore, the removal efficiency of As via the separation of Fe oxide could be increased. Furthermore, the separation of metal oxides is associated with particulates. The properties of the contaminated soil exhibited particle size dependence. The bulk soil was mainly composed of dickite, muscovite, and quartz. However, based on the XRD study, the presence of rutile TiO_2 and wustite (FeO) was verified after the removal of the small particles that were bound to the coarse particles. Toxic heavy metals can be adsorbed to small particles such as clay minerals. In particular, small particles are dominated by clay-sized phyllosilicates such as dickite and muscovite with amorphous oxides. The changes in the soil properties caused by the separation resulted in a decrease in the concentrations of the toxic heavy metals.

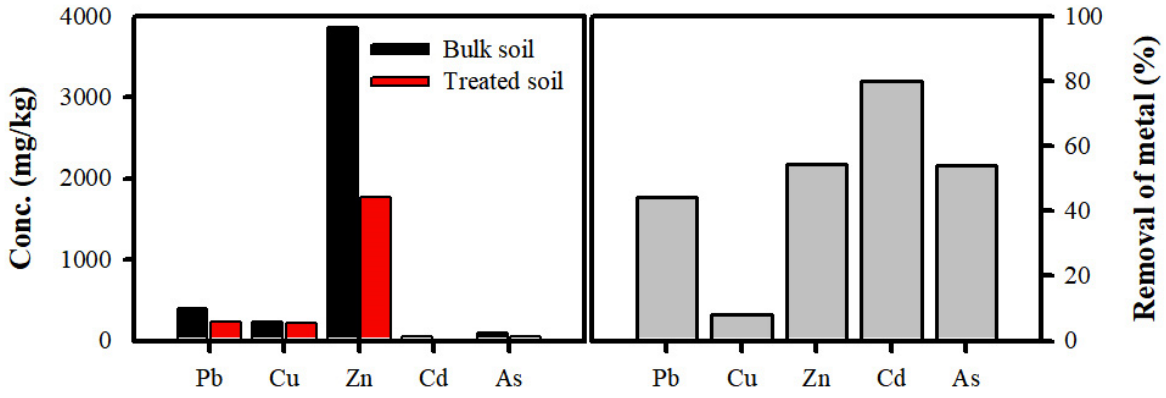

Figure 8. The toxic heavy metal concentration (mg/kg) in the bulk soil (+0.075 mm) and treated soil and removal (%) of toxic heavy metals in treated soil by a washing ejector at 5 MPa.

Figure 9 compares the altered chemical forms of the dispersed soils. The chemical forms of As in soils are associated with Fe oxide [37,38] and, by extension, the removal of As can be correlated to the separation efficiency of Fe oxide. The chemical forms of As after the separation are removed from the residual As fraction. This is likely due to the discrete particle forms that might affect the separation of the dispersed soils, given that discrete particulates present in soils can be affected by physical separation. Thus, it is associated with soil washing treatment to improve the removal of toxic heavy metals. Conversely, Pb and Zn in the soil might attribute different characteristics to the dispersed soil. The mineralogical constituents of soil are phyllosilicates such as dickite and muscovite, which are also known as clay minerals. Phyllosilicates are surrounded by amorphous oxides that can potentially bind to trace elements through specific sorption, co-precipitation, and by forming inner sphere complexes [34]. The particles that contained toxic heavy metals were composed of metal phases included in phyllosilicates, and the metal phase was weakly bound to the surface phyllosilicates or Fe oxide [19,35]. Based on the investigated chemical forms, Pb and Zn were not affected by the changes in the small particles. This suggested that trace elements were present in various solid phases depending on the surface or encapsulated in the phyllosilicates. In the separation process, collisions can occur on the surface soil, such as the metal phase that is weakly bound to surface silicate minerals. However, the removal of trace elements encapsulated in the phyllosilicates is difficult because of their mineralogical complexity.

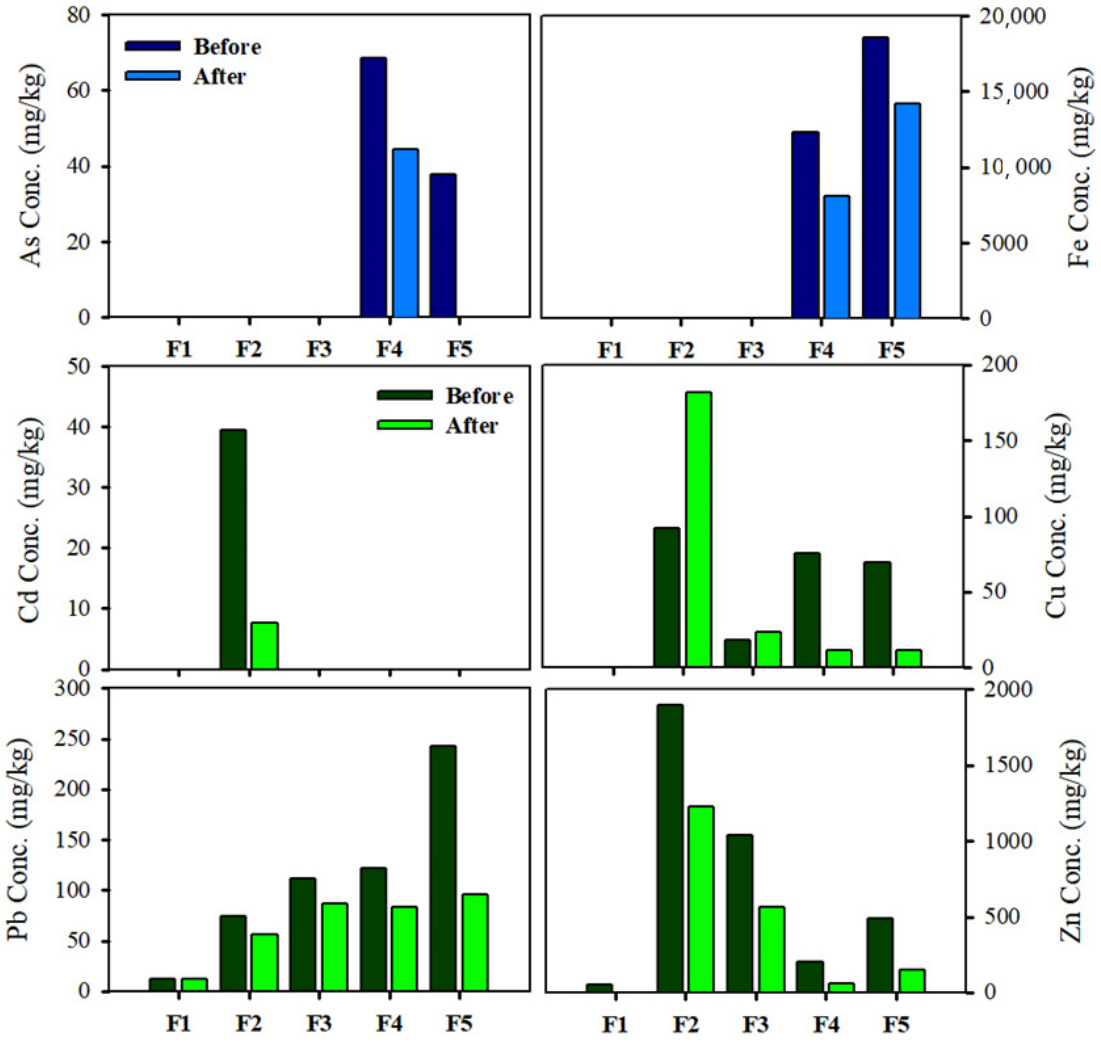

Figure 9. Sequential extracted metal fractions from bulk soil (before) and treated soil (after). For As and Fe, each fraction represents: (F1) non-specifically sorbed; (F2) specifically sorbed; (F3) amorphous oxide associated; (F4) crystalline oxide associated; (F5) residual. For Cd, Cu, Pb, and Zn, each fraction represents: (F1) exchangeable; (F2) carbonate; (F3) amorphous Fe and Mn hydroxide; (F4) organic matter bound and sulfide; (F5) residual.

4. Discussion

The bulk soil aggregates include inorganic and organic matter. Minerals in the contaminated soil comprised dickite, muscovite, and quartz. These Al- and Si-bearing minerals such as dickite and muscovite are phyllosilicate minerals of the tetrahedron and octahedron layered structures and belong to clay minerals. Overall, toxic heavy metals can either exist on the surface or be encapsulated within silicate minerals under ambient conditions. The mobility of toxic heavy metals is governed by soil properties such as Fe oxides and silicate clays [39,40]. Toxic heavy metals in contaminants can be slowly released by weathering [18,19], thereby co-precipitating metals as hydroxides and leading to occurrence of oxides of metals such as Fe, Ti, and Mn. Fe-bearing mineral phases are transformed into secondary metal species by the redox potential of the soil environment [3–5]. Fe oxide is present in various forms such as hydrous oxides (e.g., ferrihydrite, hydrohematite, and maghemite) and oxyhydroxides (e.g., goethite, lepidocrocite, and feroxyhyte). In addition, the Fe oxide phase plays a key role in the amorphous toxic heavy metal sorption process because of its reactivity, surface area, and surface charge. Moreover, clay minerals correlated with adsorption and desorption of toxic heavy metals [35,37]. Clay minerals belonging to the phyllosilicates are composed of tetrahedron and octahedron layered struc-

tures, which divide toxic heavy metal adsorption sites into surface, interlayer, and hydrate interlayer sites.

Physical separation of the contaminated soil revealed that detachment occurred due to the physicochemical properties in the clay soil components between the silicate surface and layer. One of these components is the sodium aluminum silicate surrounded by an amorphous toxic heavy metal, which revealed an increase in the intensity of the peaks through the detachment of fine particles. Further, with increasing soil particle size, several functional groups (carboxyl and hydroxyl) could be liberated, thereby detaching from clay minerals or amorphous oxides. As a result of physical separation, the efficiency of toxic heavy metal removal was greatly improved.

Overall, the treatment with the washing ejector removed organic matter and fine particles from the soil. Specifically, this treatment reduced the content of organic matter from 4.25% to 1.45%. An almost 40–60% removal efficiency of total metals (As, Zn, and Pb) was obtained from the contaminated soils. After treatment, the volume of fine particles was reduced by 28–47%. Thus, the quantity of fine particles and organic matter in larger-sized particles was reduced, which increased the intensity of the quartz peaks. Therefore, the treatment with the washing ejector could reduce the number of small particles bound to coarse particles and eliminate complex surface chemical properties (including those of soil colloids).

5. Conclusions

In this study, we used a washing ejector to separate fine particles containing contaminants originating from smelting. The washing ejector can be used to remove small particles bound to silicate minerals and disperse soil aggregates. The separation was accomplished through particle-to-particle collisions, and thus the separation efficiency was enhanced. During the separation, collisions could occur on the surface soil, such as the metal phase that was weakly bound to surface silicate minerals. In this way, the cavitating flow of fluid via a Venturi nozzle of the ejector could remove the discrete particles. The separation of the dispersed soil altered the binding of the toxic heavy metals and mineralogical characteristics. The effect of the separation on the soil aggregate showed that the changes in the soil properties were related to the changes in the quantity of oxides, organic matter, and clay minerals.

The removal of metals from the soil aggregate was largely dependent on the particle size. The overall removal of the toxic heavy metals from the coarse soil was higher than that from fine soil owing to the oxides and organic matter on the surface. When the contaminants are associated with organic matter and particulates, separation using the washing ejector can be more effective. Therefore, this type of separation improves the removal efficiency of heavy metals from soil aggregates. To remediate contaminated soil, we should determine the optimum cutoff size by considering the volume of the contaminants and the soil properties.

Author Contributions: K.C.: Writing—original draft, Writing—review and editing. H.K.: Investigation. O.P.: Methodology. N.C.: Supervision. J.L.: Conceptualization. All authors have read and agreed to the published version of the manuscript.

Funding: This study was supported by the Korea Environment Industry & Technology Institute (grant number 2020002870001).

Data Availability Statement: All data generated or analyzed during this study are included in this published article.

Conflicts of Interest: There is no conflict of interest to declare.

Appendix A

Table A1. Extraction procedures of two sequential extraction procedures.

Step (Wenzel et al., 2001) [32]	**Extractable Phase**	**Extraction Conditions**
F1	Non-specially bound	0.05 M $(NH_4)_2SO_4$
F2	Specially bound	0.05 M $(NH_4)H_2PO_4$
F3	Fe- and Al-bound amorphous hydrous oxides	0.2 M NH_4-oxalate buffer; pH 3.25
F4	Fe- and Al-bound crystalline hydrous oxides	0.2 M NH_4-oxalate buffer +0.1 M ascorbic acid; pH 3.25
F5	Residual	18 mL HNO_3 + 8 mL HF + 2 mL H_2O_2 + 2 mL H_2O
Step (Tessier et al., 1979) [33]	**Extractable Phase**	**Extraction Conditions**
F1	Exchangeable	1 M $MgCl_2$; pH 7.0
F2	Bound to carbonate	1 M NaOAc; pH 5.0
F3	Bound to amorphous Fe and Mn hydroxides	0.04 M NH_2OH-HCl in 25% (*v*/*v*) HOAc
F4	Bound to organic matter and sulfides	0.02 M HNO_3 + 5 mL of 30% H_2O_2; pH 2.0, 30% H_2O_2; pH 2, 3.2 M NH_4OAc in 20% (*v*/*v*) HN03
F5	Residual	$HClO_4$ (2 mL) + HF (10 mL), $HClO_4$ (1 mL) + HF (10 mL), $HClO_4$ (1 mL), 12 N HCl

References

1. Boente, C.; Sierra, C.; Rodríguez-Valdés, E.; Menéndez-Aguado, J.; Gallego, J. Soil washing optimization by means of attributive analysis: Case study for the removal of potentially toxic elements from soil contaminated with pyrite ash. *J. Clean. Prod.* **2017**, *142*, 2693–2699. [CrossRef]
2. Kang, M.-J.; Kwon, Y.K.; Yu, S.; Lee, P.-K.; Park, H.-S.; Song, N. Assessment of Zn pollution sources and apportionment in agricultural soils impacted by a Zn smelter in South Korea. *J. Hazard. Mater.* **2019**, *364*, 475–487.
3. Ettler, V.; Cihlová, M.; Jarošíková, A.; Mihaljevič, M.; Drahota, P.; Kříbek, B.; Vaněk, A.; Penížek, V.; Sracek, O.; Klementová, M. Oral bioaccessibility of metal (loid) s in dust materials from mining areas of northern Namibia. *Environ. Int.* **2019**, *124*, 205–215. [CrossRef] [PubMed]
4. Lee, P.-K.; Kang, M.-J.; Jeong, Y.-J.; Kwon, Y.K.; Yu, S. Lead isotopes combined with geochemical and mineralogical analyses for source identification of arsenic in agricultural soils surrounding a zinc smelter. *J. Hazard. Mater.* **2020**, *382*, 121044. [CrossRef]
5. Ettler, V. Soil contamination near non-ferrous metal smelters: A review. *Appl. Geochem.* **2016**, *64*, 56–74. [CrossRef]
6. Lee, P.-K.; Kang, M.-J.; Yu, S.; Kwon, Y.K. Assessment of trace metal pollution in roof dusts and soils near a large Zn smelter. *Sci. Total Environ.* **2020**, *713*, 136536. [CrossRef]
7. Cho, K.; Kang, J.; Kim, S.; Purev, O.; Myung, E.; Kim, H.; Choi, N. Effect of inorganic carbonate and organic matter in thermal treatment of mercury-contaminated soil. *Environ. Sci. Pollut. Res.* **2021**, *28*, 48184–48193. [CrossRef]
8. Liao, X.; Li, Y.; Yan, X. Removal of heavy metals and arsenic from a co-contaminated soil by sieving combined with washing process. *J. Environ. Sci.* **2016**, *41*, 202–210. [CrossRef]
9. Oh, C.; Rhee, S.; Oh, M.; Park, J. Removal characteristics of As (III) and As (V) from acidic aqueous solution by steel making slag. *J. Hazard. Mater.* **2012**, *213*, 147–155. [CrossRef]
10. Im, J.; Yang, K.; Jho, E.H.; Nam, K. Effect of different soil washing solutions on bioavailability of residual arsenic in soils and soil properties. *Chemosphere* **2015**, *138*, 253–258. [CrossRef]
11. Li, Y.; Liao, X.; Li, W. Combined sieving and washing of multi-metal-contaminated soils using remediation equipment: A pilot-scale demonstration. *J. Clean. Prod.* **2019**, *212*, 81–89. [CrossRef]
12. Andreozzi, R.; Fabbricino, M.; Ferraro, A.; Lerza, S.; Marotta, R.; Pirozzi, F.; Race, M. Simultaneous removal of Cr(III) from high contaminated soil and recovery of lactic acid from the spent solution. *J. Environ. Manag.* **2020**, *268*, 110584. [CrossRef]
13. Bianco, F.; Race, M.; Papirio, S.; Oleszczuk, P.; Esposito, G. The addition of biochar as a sustainable strategy for the remediation of PAH-contaminated sediments. *Chemosphere* **2021**, *263*, 128274. [CrossRef]
14. Lee, J.-I.; Kang, J.-K.; Oh, J.-S.; Yoo, S.-C.; Lee, C.-G.; Jho, E.H.; Park, S.-J. New insight to the use of oyster shell for removing phosphorus from aqueous solutions and fertilizing rice growth. *J. Clean. Prod.* **2021**, *328*, 129536. [CrossRef]
15. Kominkova, D.; Fabbricino, M.; Gurung, B.; Race, M.; Tritto, C.; Ponzo, A. Sequential application of soil washing and phytoremediation in the land of fires. *J. Environ. Manag.* **2018**, *206*, 1081–1089. [CrossRef] [PubMed]
16. Dermont, G.; Bergeron, M.; Mercier, G.; Richer-Laflèche, M. Soil washing for metal removal: A review of physical/chemical technologies and field applications. *J. Hazard. Mater.* **2008**, *152*, 1–31. [CrossRef] [PubMed]

17. Lin, R.; Howard, B.H.; Roth, E.A.; Bank, T.L.; Granite, E.J.; Soong, Y. Enrichment of rare earth elements from coal and coal by-products by physical separations. *Fuel* **2017**, *200*, 506–520. [CrossRef]
18. Ko, I.; Chang, Y.-Y.; Lee, C.-H.; Kim, K.-W. Assessment of pilot-scale acid washing of soil contaminated with As, Zn and Ni using the BCR three-step sequential extraction. *J. Hazard. Mater.* **2005**, *127*, 1–13. [CrossRef] [PubMed]
19. Kim, E.J.; Yoo, J.-C.; Baek, K. Arsenic speciation and bioaccessibility in arsenic-contaminated soils: Sequential extraction and mineralogical investigation. *Environ. Pollut.* **2014**, *186*, 29–35. [CrossRef]
20. Ma, J.; Lei, M.; Weng, L.; Li, Y.; Chen, Y.; Islam, M.S.; Zhao, J.; Chen, T. Fractions and colloidal distribution of arsenic associated with iron oxide minerals in lead-zinc mine-contaminated soils: Comparison of tailings and smelter pollution. *Chemosphere* **2019**, *227*, 614–623. [CrossRef]
21. Li, M.; Bussonnière, A.; Bronson, M.; Xu, Z.; Liu, Q. Study of Venturi tube geometry on the hydrodynamic cavitation for the generation of microbubbles. *Miner. Eng.* **2019**, *132*, 268–274. [CrossRef]
22. Shi, H.; Li, M.; Nikrityuk, P.; Liu, Q. Experimental and numerical study of cavitation flows in venturi tubes: From CFD to an empirical model. *Chem. Eng. Sci.* **2019**, *207*, 672–687. [CrossRef]
23. Musmarra, D.; Prisciandaro, M.; Capocelli, M.; Karatza, D.; Iovino, P.; Canzano, S.; Lancia, A. Degradation of ibuprofen by hydrodynamic cavitation: Reaction pathways and effect of operational parameters. *Ultrason. Sonochem* **2016**, *29*, 76–83. [CrossRef]
24. Nie, G.; Hu, K.; Ren, W.; Zhou, P.; Duan, X.; Xiao, L.; Wang, S. Mechanical agitation accelerated ultrasonication for wastewater treatment: Sustainable production of hydroxyl radicals. *Water Res.* **2021**, *198*, 117124. [CrossRef] [PubMed]
25. Wang, B.; He, R.; Chen, M.; Pi, S.; Zhang, F.; Zhou, A.; Zhang, Z. Intensification on mass transfer between gas and liquid in fine bubble jet reactor. *J. Environ. Chem. Eng.* **2021**, *9*, 104718. [CrossRef]
26. Song, L.; Yang, J.; Yu, S.; Xu, M.; Liang, Y.; Pan, X.; Yao, L. Ultra-high efficient hydrodynamic cavitation enhanced oxidation of nitric oxide with chlorine dioxide. *Chem. Eng. J.* **2019**, *373*, 767–779. [CrossRef]
27. Fang, L.; Xu, X.; Li, A.; Wang, Z.; Li, Q. Numerical investigation on the flow characteristics and choking mechanism of cavitation-induced choked flow in a Venturi reactor. *Chem. Eng. J.* **2021**, *423*, 130234. [CrossRef]
28. Hung, C.M.; Huang, C.P.; Chen, C.W.; Dong, C.D. Hydrodynamic cavitation activation of persulfate for the degradation of polycyclic aromatic hydrocarbons in marine sediments. *Environ. Pollut.* **2021**, *286*, 117245. [CrossRef]
29. Bermejo, D.; Escaler, X.; Ruíz-Mansilla, R. Experimental investigation of a cavitating Venturi and its application to flow metering. *Flow Meas. Instrum.* **2021**, *78*, 101868. [CrossRef]
30. Shi, H.; Li, M.; Liu, Q.; Nikrityuk, P. Experimental and numerical study of cavitating particulate flows in a Venturi tube. *Chem. Eng. Sci.* **2020**, *219*, 115598. [CrossRef]
31. Badve, M.; Gogate, P.; Pandit, A.; Csoka, L. Hydrodynamic cavitation as a novel approach for wastewater treatment in wood finishing industry. *Sep. Purif. Technol.* **2013**, *106*, 15–21. [CrossRef]
32. Wenzel, W.W.; Kirchbaumer, N.; Prohaska, T.; Stingeder, G.; Lombi, E.; Adriano, D.C. Arsenic fractionation in soils using an improved sequential extraction procedure. *Anal. Chim. Acta* **2001**, *436*, 309–323.
33. Tessier, A.; Campbell, P.G.; Bisson, M. Sequential extraction procedure for the speciation of particulate trace metals. *Anal. Chem.* **1979**, *51*, 844–851. [CrossRef]
34. Jeong, S.; Hong, J.K.; Jho, E.H.; Nam, K. Interaction among soil physicochemical properties, bacterial community structure, and arsenic contamination: Clay-induced change in long-term arsenic contaminated soils. *J. Hazard. Mater.* **2019**, *378*, 120729. [CrossRef] [PubMed]
35. Kim, E.J.; Baek, K. Enhanced reductive extraction of arsenic from contaminated soils by a combination of dithionite and oxalate. *J. Hazard. Mater.* **2015**, *284*, 19–26. [CrossRef]
36. Ettler, V.; Chren, M.; Mihaljevič, M.; Drahota, P.; Kříbek, B.; Veselovský, F.; Sracek, O.; Vaněk, A.; Penížek, V.; Komárek, M. Characterization of Fe-Mn concentric nodules from Luvisol irrigated by mine water in a semi-arid agricultural area. *Geoderma* **2017**, *299*, 32–42. [CrossRef]
37. Xu, J.; Kleja, D.B.; Biester, H.; Lagerkvist, A.; Kumpiene, J. Influence of particle size distribution, organic carbon, pH and chlorides on washing of mercury contaminated soil. *Chemosphere* **2014**, *109*, 99–105. [CrossRef]
38. Qi, Y.; Zhang, T.C. Sorption of testosterone on partially-dispersed soil particles of different size fractions: Methodology and implications. *Water Res.* **2016**, *92*, 1–10. [CrossRef] [PubMed]
39. Siddiqui, S.I.; Chaudhry, S.A. Iron oxide and its modified forms as an adsorbent for arsenic removal: A comprehensive recent advancement. *Process Saf. Environ. Prot.* **2017**, *111*, 592–626. [CrossRef]
40. Yang, K.; Kim, B.-C.; Nam, K.; Choi, Y. The effect of arsenic chemical form and mixing regime on arsenic mass transfer from soil to magnetite. *Environ. Sci. Pollut. Res.* **2017**, *24*, 8479–8488. [CrossRef]